This is a peer-reviewed, author's accepted manuscript of the following research article: Riaz, F., Hossain, M. S., Roney, M., Ali, Y., Qureshi, S., Muhammad, R., Abd Hamid, S., Seidel, V., ur Rashid, H., & Chiau Ming, L. (2022). Evaluation of potential bacterial protease inhibitor properties of selected hydroxyquinoline derivatives: an in silico docking and molecular dynamics simulation approach. *Journal of Biomolecular Structure and Dynamics*, 1-14. https://doi.org/10.1080/07391102.2022.2146200

Evaluation of Potential Bacterial Protease Inhibitor Properties of Selected Hydroxyquinoline Derivatives: an *in Silico* Docking and Molecular Dynamics Simulation Approach

Faiza Riaz [1‡], Md. Sanower Hossain [2‡*], Miah Roney [3‡], Yousaf Ali [4,*], Saira Qureshi [1], Riaz Muhammad [1], Said Moshawih [5], Shafida Abd Hamid [6], Veronique Seidel [7], Haroon ur Rashid [8] and Long Chiau Ming [5]

[1] Department of Chemistry, Sarhad University of Science and Information Technology, Peshawar, Pakistan; faizariaz59@gmail.com (F.R.); sairaqureshi068@gmail.com (S.Q.); riazm.chemistry@suit.edu.pk (R.M.)

[2] Centre for Sustainability of Ecosystem and Earth Resources (Pusat ALAM), Universiti Malaysia Pahang, Kuantan 26300, Malaysia; mshossainbge@gmail.com

[3] Faculty of Industrial Sciences and Technology, Universiti Malaysia Pahang, Lebuhraya Tun Razak, 26300 Gambang, Kuantan, Pahang Darul Makmur, Malaysia; saroney35@gmail.com

[4] Faculty of Allied Health Sciences, Iqra National University Swat Campus, Khyber Pakhtunkhwa Pakistan; yousaf.chemistry@suit.edu.pk

[5] PAP Rashidah Sa'adatul Bolkiah Institute of Health Sciences, Universiti Brunei Darus-salam, Gadong, BE1410 Brunei Darussalam; saeedmomo@hotmail.com (S.M.) long.ming@ubd.edu.bn (L.C.M.)

[6] Kulliyyah of Science, International Islamic University Malaysia, 25200 Kuantan, Pahang Malaysia; shafida@iium.edu.my

[7] Natural Products Research Laboratory, Strathclyde Institute of Pharmacy and Biomedical Sciences, University of Strathclyde, Glasgow G4 0RE, UK; veronique.seidel@strath.ac.uk

[8] Institute of Chemistry, Federal University of Mato Grosso do Sul, Campo Grande, MS, Brazil; haroongold@gmail.com

‡Authors contributed equally and shared the first-author position

*Correspondence: mshossainbge@gmail.com (M.S.H.); yousaf.chemistry@suit.edu.pk (Y.A.); Tel.: +92 343 9585007 (Y.A.); +601169609649 (M.S.H.)

Abstract: Antimicrobial drug resistance (AMR) is a severe global threat to public health. The increasing emergence of drug-resistant bacteria requires the discovery of novel antibacterial agents. Quinoline derivatives have previously been reported to exhibit antimalarial, antiviral, antitumor, antiulcer, antioxidant, and, most interestingly, antibacterial properties. In this study, we evaluated the binding affinity of three newly designed hydroxyquinolines derived from sulfanilamide (**1**), 4-amino benzoic acid (**2**), and sulfanilic acid (**3**) towards five bacterial protein targets (PDB ID: 1JIJ, 3VOB, 1ZI0, 6F86, 4CJN). The three derivatives were designed considering the amino acid residues identified at the active site of each protein involved in the binding of each co-crystallized ligand and drug-likeness properties. The ligands displayed binding energy values with the target proteins ranging from −2.17 to −8.45 kcal/mol. Compounds (**1**) and (**3**) showed the best binding scores towards 1ZI0/3VOB and 1JIJ/4CJN, respectively, which may serve as new antibiotic scaffolds. Our *in silico* results suggest that sulfanilamide (**1**) or sulfanilic acid (**3**) hydroxyquinoline derivatives have the potential to be developed as bacterial inhibitors, particularly MRSA inhibitors. But before that, it must go through the proper preclinical and clinical trials for

further scientific validation. Further experimental studies are warranted to explore the antibacterial potential of these compounds through preclinical and clinical studies.

Keywords: Antibacterial agents; Hydroxyquinolines; Molecular docking; ADMET; Drug-likeness; *In-silico*.

Introduction

Infections remain one of the major threats to human health, and combatting infectious diseases has become a challenge worldwide (M. S. Hossain et al., 2021; S. Hossain et al., 2021; Sharma et al., 2018; Urbi et al., 2021). The human and economic costs of infections caused by bacteria, in particular, are a growing cause of concern (Muthukumar et al., 2019). Several bacterial pathogens have developed resistance to antibiotics, including strains identified as multi- or extensively-drug-resistant (El Faydy et al., 2017; Karuniawati et al., 2021). The Gram-positive bacterium Methicillin-resistant *Staphylococcus aureus* (MRSA) can cause skin, soft tissue, bone, joint infections, endocarditis, and septicemia is a typical example of a drug-resistant microorganism (Qiu et al., 2001; Solomon & Oliver, 2014; Tjampakasari et al., 2021). Gram-negative bacteria also cause significant morbidity and mortality worldwide; several strains have also become drug-resistant (Breijyeh et al., 2020).

S. aureus infections are a global concern due to their high rate of developing antimicrobial resistance (AMR), limiting therapeutic options, and healthcare-associated infections. The all-cause mortality rate, particularly from *S. aureus* bacteremia in the developed countries, reached up to 20–30%, with even over 50% rates in some less- and average-developing countries (Nakajima et al., 1978). The leading cause of AMR development is either one of them: (i) alteration of target,

(ii) inactivation of antibiotic, (iii) bypass antibiotic, and (iv) restricted antibiotic accumulation. Additionally, this process accelerated because of the misuse and overuse of antibiotics and poor infection prevention and control (Karuniawati et al., 2021; WHO, 2020). There are multiple enzymes involved in the development of AMR. For example, DNA gyrases (type II topoisomerases), aminoacyl-tRNA synthetases, adenylate kinases, *Penicillin*-Binding Proteins (PBPs), isomaltase, and the FtsZ protein (Sashidhara et al., 2015). These enzymes are important in surviving or producing offspring and are commonly found in many microbial species. For example, aminoacyl-tRNA synthetases catalyzed the esterification of the amino acid to their cognate tRNAs, which are necessary for decoding the genetic information during protein synthesis (Qiu et al., 2001). All of these enzymes can be a target for drug discovery of antimicrobial agents.

Heterocyclic molecules have played an important role in developing various therapeutic agents to date, including a range of antibacterial drugs (Mustafa, 2018). The quinoline moiety is prevalent in a large number of compounds (Mandewale et al., 2015). Quinoline derivatives can engage in nucleophilic as well as electrophilic substitution reactions (Le et al., 2018). In 8-hydroxyquinolines, introducing substituents at the C-5, C-7, and/or C-8 positions have been identified as an attractive approach to developing more biologically-active drugs (Faydy et al., 2021). Quinoline derivatives have been reported to exhibit antimalarial, antiviral, antitumor, antiulcer, antioxidant and, most interestingly, antibacterial properties (Kouznetsov et al., 2020; T. O. Kumar et al., 2015). Its derivatives have been characterized as inhibitors of bacterial proteins, including DNA gyrases, aminoacyl-tRNA synthetases, adenylate kinases, PBPs, isomaltase, and the FtsZ protein (Sashidhara et al., 2015). Many recent studies synthesized several hydroxyquinoline derivatives, and experimental investigations have shown potential antimicrobial activities against many pathogenic bacteria, such as *E. coli*, *S. aureus*, *V. parahaemolyticus*, and

P. aeruginosa, and fungi, such as *Candida* spp. (Cherdtrakulkiat et al., 2016; El Faydy et al., 2017; Enquist et al., 2012; Joaquim et al., 2021; Lam et al., 2014; Mohamed Rbaa et al., 2019; M. Rbaa et al., 2019). Some of these derivates designed based on the 8- hydroxyquinoline, including sulfanilamide (**1**)**,** 4-*p*-amino benzoic acid (**2**), and sulfanilic acid (**3**) (Figure 1), might have potential antibacterial properties. These three compounds have therapeutically important diverse functional groups. All the compounds have a low molecular weight (less than 500 g/mol), and contain a certain degree of flexibility, and hence considered closer to Lipinski's rule of 5. According to Ezeokonkwo et al. (Ezeokonkwo et al., 2019), the presence of different substituents around the 8-hydroxyquinoline nucleus, such as amine, sulfa groups halogen, hydroxyl or thiol group at the position-5 of the 8-hydroxy quinoline ring, gives rise to improved inhibiting bacterial infections via binding to DNA and display DNA photocleavage activity. Variation at position-5 results in hydrogen bonding and hydrophobic interaction with the active site protein residues (Mandewale et al., 2015). P-aminobenzoic acid (PABA) is structurally similar to Sulfonamides. This compound can fit into the receptor protein's active site and inhibit bacterial infections. This structural similarity of PABA enables competitive inhibition of dihydropteroate synthase (DHPS). PABA analogue is considered a keystone in treating infections (Thiede et al., 2016). Keeping in view the characteristic features of the selected incorporated quinoline nucleus in the designed antibacterial drugs act as DNA gyrase inhibitors and efflux pumps inhibitor in bacteria. To increase the selected compounds' drug-like properties, we designed and introduced pharmacophores (sulfanilamide, PABA, and sulfonic acid) at position-5 on the quinoline nucleus.

Docking's study applies computer-based models to predict the best-fit orientation of a ligand (new chemical entity or drugs) that binds to a particular receptor of interest. It is widely used to predict the preferred direction of the designed molecule to a receptor when bound to each other to form a

stable complex (P. Gupta et al., 2019). In the field of pharmacology, these studies could help predict the conformation of drugs (ligands) in the active site of the particular receptor of interest, which can provide a better understanding of the complexity of living systems (M. Gupta et al., 2018). In the light of discovering antibacterial agents, this study evaluated three hydroxyquinoline derivatives, namely sulfanilamide (**1**)**,** PABA (**2**), and sulfanilic acid **(3**) (Figure 1), as inhibitors of five known antimicrobial receptors, namely tyrosyl-tRNA synthetase and an FtsZ protein from *S. aureus*, DNA gyrases from *E. coli* and a PBP2a from MRSA by molecular docking and molecular dynamics simulation study to validate the results. Derivatives with the highest affinity were then compared with co-crystallized compounds to determine the level of similarity of amino acid interactions that occur, indicating this potential as an antimicrobial compound. Moreover, an *in-silico* study was performed to predict the ADMET and drug-likeness properties of the hydroxyquinoline derivatives.

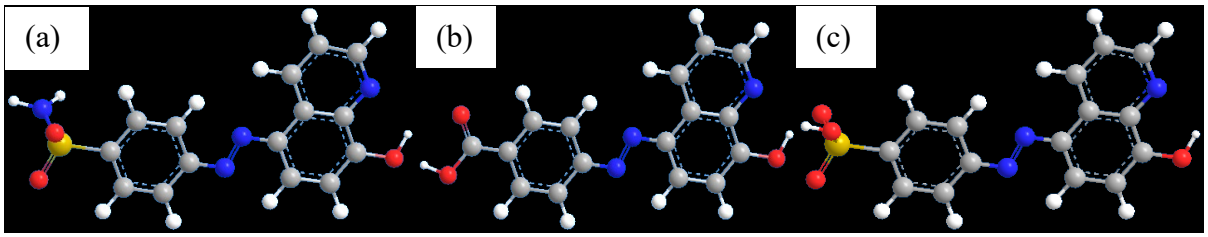

Figure 1. Structure of three hydroxyquinoline derivatives with (a) sulfanilamide (**1**), (b) 4-p-amino benzoic acid (**2**), and (c) sulfanilic acid (**3**) moieties. Red: Oxygen, Grey: Carbon, Blue: Nitrogen, White: Hydrogen, and Golden: Sulfur.

Materials and Methods

Bacterial protein and ligand preparation

The three-dimensional (3D) crystal structures of five bacterial proteins (PDB ID: 1JIJ, 3VOB, 1ZI0, 6F86, 4CJN) were used for docking. The 3D structures of all proteins, in complex with their respective co-crystallized ligands, were downloaded from the RCSB Protein Data Bank (https://www.rcsb.org/). Each protein was prepared for docking using the Auto Preparation tool of AutoDock 4.2 (MGLTools 1.5.6). All water molecules and hetero atoms were removed, and polar hydrogens and Kollman charges were added. The active binding site residues of each protein were determined using CASTEP.

Three hydroxyquinoline derivatives with **1, 2**, and **3** moieties were designed as potential ligands for this study (Figure 1). Their 3D structures were drawn with the correct stereochemistry, and energy minimization was run for each ligand using ChemSketch. AutoDock Tools 4.2 was used to prepare the ligands for the docking, assigning Gasteiger charges and correcting bond orders.

Molecular docking

The docking software supplied with AutoDock4.2 and AutoGrid4.2 was used to obtain grid maps. The size of the grid box (60, 60, and 60 points in x, y, and z directions) was built with a grid spacing of 0.375 Å using a graphical user interface program so as to contain the binding sites of each target protein. About 10 conformers for each ligand were used in the docking algorithm to rank the most suitable conformation of the ligand in the active site of each protein. The conformations with minimum free binding energy (ΔG bind) were compared with those obtained for the respective co-crystallized ligands (controls). To improve the energy evaluation, a Lamarckian genetic algorithm (LGA) was chosen for the docking. All results were assessed by analyzing the Root Mean Square Deviation (RMSD) values, the binding energy (ΔG bind), ligand-

protein interactions, and the number of current conformations in a cluster. All molecular interactions were visualized using BIOVA Discovery Studio Visualizer.

Prediction of ADMET and drug-likeness properties

The pharmacokinetic properties were predicted using pkCSM online software (http://biosig.unimelb.edu.au/pkcsm/). pkCSM is an online website that allows the user to draw their respective ligand or drug molecule or include SMILES data from PubChem and provides the parameters such as Aqueous Solubility, Human Intestine Absorption, Blood Brain Barrier, CYP Substrate, CYP Inhibitor, hERG and Hepatotoxicity (Enmozhi et al., 2021). Moreover, Drug-likeness predictions were determined using previously established rules/parameters, including Lipinski's rule of five, Veber's rule, Ghose rule, and Egan rule (Berry & Phillips, 1998).

Molecular Dynamic (MD) Simulation

The protein-ligand complexes from the respective target species were immersed in the predefined water (TIP3P) as a solvent in the orthorhombic box of the size 10 Å × 10 Å × 10 Å with periodic boundary conditions. The system was neutralized with salt (Na^+ and Cl^-) at 0.15 M concentration. The prepared system was then submitted to the final molecular dynamic simulation for 100 ns, and the trajectory sampling was done at an interval of 10.0 ps. During the simulations, the system was relaxed in a stepwise manner using the protocols of Steepest Descent and the limited-memory Broyden-Fletcher-Goldfarb-Shanno (LBFGS) algorithms. The simulations were conducted with a constant temperature of 300.0 K using a Nosé-Hoover chain thermostat (Oh & Klein, 2006) and Martyna-Tobias-Klein barostat methods (Neupane et al., 2022) at one atm of pressure with

isotropic coupling type. The short-range and long-range coulumb interactions were analyzed using a cut-off value of 9.0 Å and the particle mesh Ewald method (Liang et al., 2021), respectively. The final production run was carried out for 10 ns, and the trajectory sampling was done at an interval of 1.0 ps.

Molecular mechanics generalized Born surface area (MM/GBSA) calculations

MMGBSA can be performed to calculate ligand binding free energies and ligand strain energies for a set of ligands and a single receptor (Genheden & Ryde, 2010; Godschalk et al., 2013). After completing the interaction binding affinity analysis, the MMGBSA was conducted by utilizing the Prime model of Schrödinger suite 2020-3 (Maestro Application, Paid Version). We have analyzed the relative binding free affinity of ligand **2** with 1ZIO protein complex, **3** with 1JIJ protein complex, and **3** with 3VOB protein complex.

Results and Discussion

Docking with 1JIJ

The key amino acid residues at the active site of 1JIJ were identified as Asp151, Asp195, Asp177, Asp80, Asn199, Gln196, Gly193, Gln174, Tyr170, Asp180, Leu70, His50, Gly49, Asp40, Ala39, Gly38, and Tyr36. The predicted binding energies, inhibition constant (Ki) values and molecular interactions of ligands (**1-3**) with the 1JIJ protein target are given in Table 1. The lowest binding energy (−8.48 kcal/mol) and the lowest Ki (1.11 μM) were obtained for compound (**3**). Compound (**3**) interacted with H-B with the residues of Tyr36, Asp40, and Arg88. Moreover, this compound interacted with strong π-alkyl bonds with Leu70, Ala39, and Cys37 residues. According to the published work by Bouzian et al. (Y. Bouzian et al., 2020), the best binding energy for 1JIJ was

observed in mode 1 with an energy of -6.9 kcal/mol) and three hydrogen bonding interactions. These values were better than those obtained for chloramphenicol (co-crystallized ligand control).

The detailed interactions between **3** and IJIJ are shown in Table 2 and Figure 2. Interactions observed for **1** and **2** are presented in the Supplementary Material (Figure S1, S2). 1JIJ, a tyrosyl-tRNA synthetase from *S. aureus*, plays an important role in protein biosynthesis by producing charged transfer RNAs. If this enzyme is inhibited, protein synthesis is impaired, subsequently impairing bacterial growth (Berry & Phillips, 1998; Jin et al., 2020). Previous molecular docking studies have revealed two quinoline derivatives, namely dodecyl 2-(dodecyloxy) quinoline-4-carboxylate, and dodecyl 1-dodecyl-2-oxo-1,2-dihydroquinoline-4-carboxylate, had high affinity for 1JIJ (Younos Bouzian et al., 2020). The same study also showed that dodecyl 2-(dodecyloxy) quinoline-4-carboxylate displayed antibacterial activity against *S. aureus* (MIC of 6.25 µg/mL) (Younos Bouzian et al., 2020). The strong binding score obtained for **3** in our study suggests that this quinoline derivative may serve as a potential template for new anti-*Staphylococcal* agents.

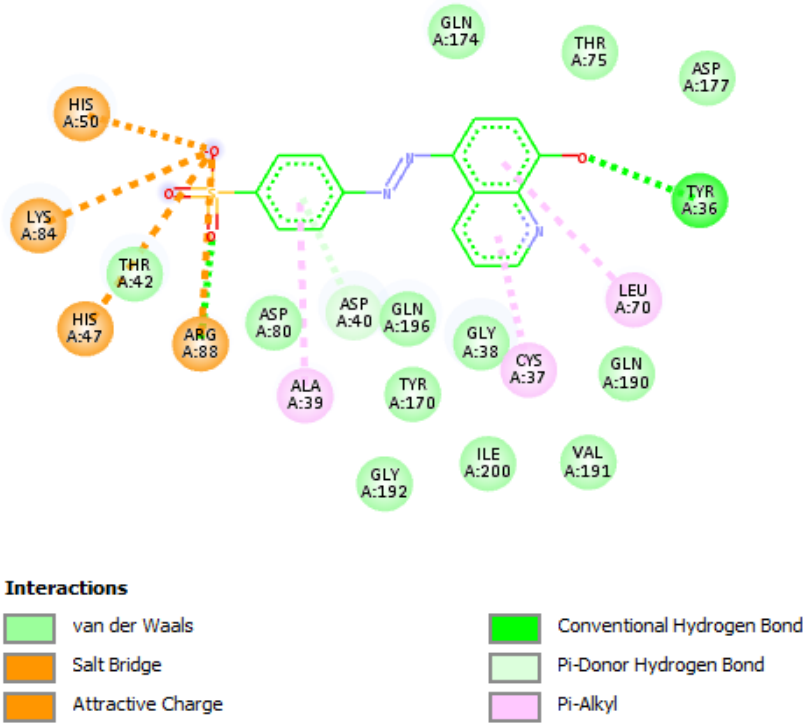

Figure 2. Docked pose of **3** in the 1JIJ binding site showing molecular interactions

Docking with 3VOB

The key amino acid residues at the active site of 3VOB were identified as Leu200, Val297, Val203, Gly193, Gly196, Ile197, Thr309, Ile331, Gln192, Gly227, Met226, and Ile228. The predicted binding energies, inhibition constant (Ki) values and molecular interactions of ligands (**1-3**) with the 3VOB protein target are given in Table 3. The lowest binding energy (−8.54 kcal/mol) and the lowest Ki (1.00 μM) were obtained for **3**, while in literature, binding energies for 3VOB are in the range of -5.89 to -8.32 for a series of derivatives (Faydy et al., 2021). These values were better than those obtained for nitroxoline (co-crystallized ligand control).

Detailed interactions between **3** and 3VOB are shown in Figure 4 and Table 4. In this study, the residual amino acid interactions of synthesized ligands with DNA gyrase (6f86) were well in agreement with the previously reported binding. According to Figure 3, **3** interacts through the hydrogen bond interactions with Thr309. This compound also shows the π-sigma interactions with Val297. Leu200, Val309, and Val297 by the π-alkyl interactions. It has been shown that these binding fixes the movement and may prevent the active residues from being located at the appropriate site and act as an inhibitor, expressing anti-*Staphylococcal* activity. It is a promising candidate for medicine against *S. aureus*. Interactions observed for **1** and **2** are presented in the supplementary material (Figure S3, S4). 3VOB is an FtsZ protein from *S. aureus* that works as a prokaryotic analogue of the eukaryotic protein tubulin and is crucial for bacterial cell division (Adams & Errington, 2009; Oliva et al., 2004). The strong binding score obtained for **3** indicates its potentiality against *S. aureus* and this compound might be serve as a potential template for new anti-*Staphylococcal* agents.

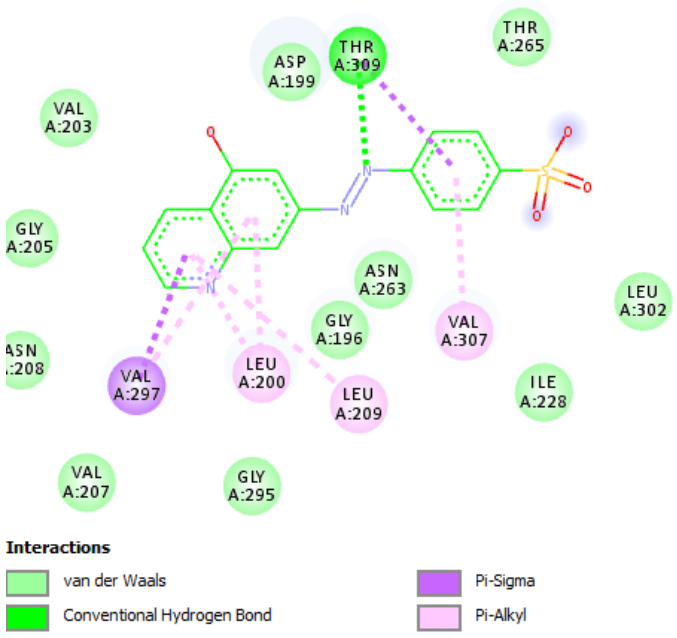

Figure 3. Docked pose of **3** in the 3VOB binding site showing molecular interactions

Docking with 1ZI0

The key amino acid residues at the active site of 1ZI0 were identified as Leu735, Gln788, Asp686, Ser734, Val737, Val787, Arg739, Val685, Leu836, and Val784. The predicted binding energies, inhibition constant (Ki) values and molecular interactions of ligands (**1-3**) with the 1ZI0 protein target are given in Table 5. The lowest binding energy (−9.08 kcal/mol) and the lowest Ki (0.22 μM) were obtained for **2**. These values were better as compared to the values mentioned in the literature. The binding energies for 1ZIO in the literature ranged from -6.7 kcal/mol to -8.88 kcal/mol (Abdullah et al., 2014).

Detailed interactions between **2** and IZI0 are shown in Figure 6 and Table 6. Compound **2** interacted hydrogen bond with Asp686 and Arg838, one pi-sigma bond with Ile736 and two pi-alkyl bonds with Leu735 and Val787 residues. Interactions observed for compounds **1** and **3** are

presented in the supplementary material (Figure S5, S6). IZI0 is a DNA gyrase (type A) present in *E. coli* and responsible for preserving the correct level of supercoiling in bacterial DNA (Narramore et al., 2019). This study is the first to report the strong binding affinity of a quinoline derivative for *E. coli* DNA gyrase (type A). Compound **1** may be served as a potential template for new drugs against the Gram-negative *E. coli.*

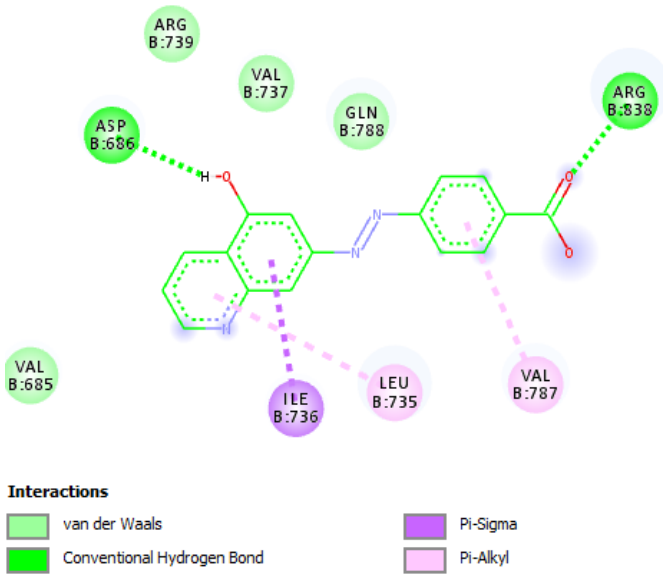

Figure 4. Docked pose of **2** in the IZI0 binding site showing molecular interactions

Docking with 6F86

The key amino acid residues at the active site of 6F86 were identified as Val43, Val71, Ile78, Ala47, Ile94, Asp73, Arg76, Ala47, Glu50, Gly77, Pro79, Gly75, Thr165, and Val120. The predicted binding energies, inhibition constant (Ki) values, and molecular interactions of ligands (**1-3**) with 6F86 are given in Table 7. This protein target is a DNA gyrase (type B) present in *E. coli* and responsible for preserving the correct level of supercoiling in bacterial DNA (Zeleke et al., 2020). Compound **3** showed better binding affinity than the co-crystallized ligand, and the Ki

value is comparable. This compound interacted with hydrogen bonds with Asn46, Asp73, and Val120 residues. Moreover, compound **3** showed pi-sigma interaction with Ile78 and Thr165 residues, as well as one amide-pi stacked with Asn46 and two pi-alkyl bonds with Ile78 and Ile94 amino acid residues. The interactions observed for all ligands are presented in the supplementary material (Figure S7-S9).

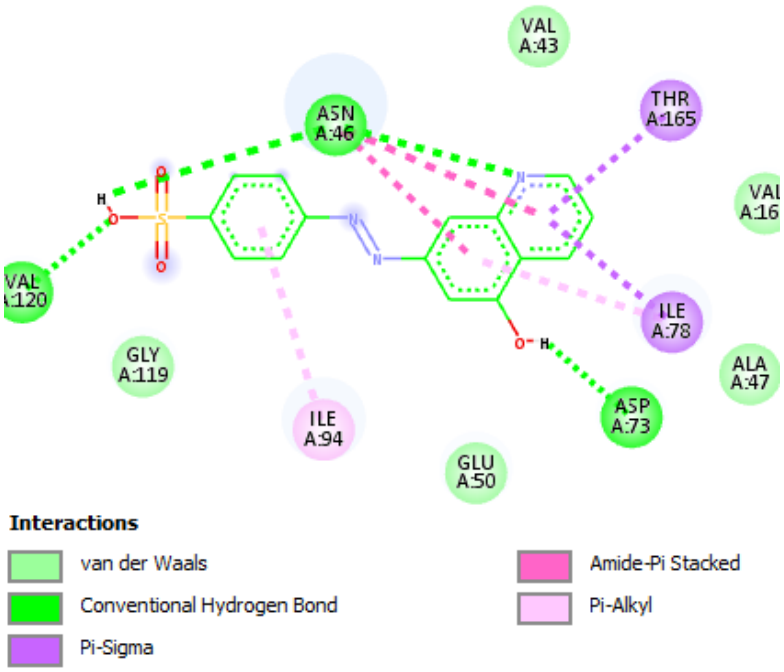

Figure 5. Docked pose of **3** in the 6F86 binding site showing molecular interactions.

Docking with 4CJN

The key amino acid residues at the active site of 4CJN were identified as Pro401, Gly402, Ser403, Lys406, Tyr446, Ser461, Ser462, Asp463, Asn464, Ile465, Phe466, Tyr519, Gly520, Gln521, Ser598, Gly599, Thr600, Ala601, Glu602, Leu603, Arg612, Gln613, Ile614, and Ala642. The predicted binding energies, inhibition constant (Ki) values and molecular interactions of ligands (**1-3**) with 4CJN are given in Table 8. The lowest binding energy (−8.45 kcal/mol) and the lowest

Ki (0.88 µM) were obtained for **3**. Compound **3** projected two hydrogen bonds with Ser403 and Ser462 residues. Moreover, this compound showed one hydrophobic interaction with the residues of Gly599 and one strong pi-alkyl bond with the Ala462 residue. These values were better than those obtained for ceftaroline (co-crystallized ligand control).

Detailed interactions between **3** and 4CJN are shown in Figure 5 and Table 9. Interactions observed for compounds **1** and **2** are presented in the supplementary material (Figure S10, S11). 4CJN is a Penicillin-Binding Protein (PBP2a) in MRSA that plays the primary role in the biosynthesis of the bacterial cell wall (V. Kumar et al., 2020). This study is the first to report the strong binding affinity of a quinoline derivative for the PBP2a of MRSA. Compound **3** may serve as a potential template for new drugs against MRSA.

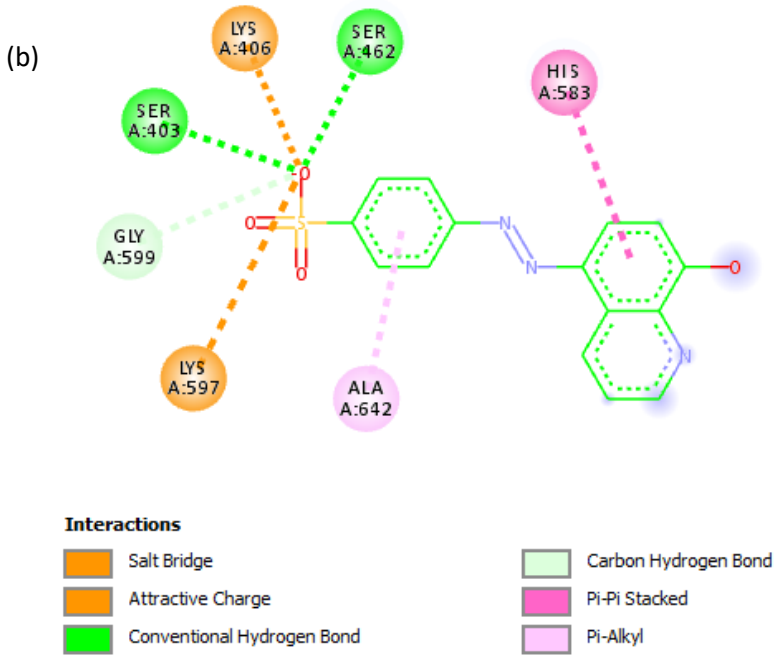

Figure 6. Docked pose of **3** in the 4CJN binding site showing molecular interactions

Table 1. Predicted binding energy (ΔG bind) and inhibition constant (Ki) values of three hydroxyquinolines derived from the selected bacterial proteins

Compound Number	PDB ID	ΔG bind (kcal/mol)	Ki (μM)	Amino Acids
Chloramphenicol	1JIJ	-6.88	9.0	Cys37, Gly38, Asp80, Lys84, Arg88, Gly193 (H-B), Asp80 (Pi-anion), Cys37, Ala39, His50, Pro53, Phe54 (alkyl/pi-alkyl)
Compound (**3**)		-8.48	1.11	Tyr36, Asp40, Arg88 (H-B), Leu70, Ala39, Cys37 (pi-alkyl), His47, His50, Lys84, Arg88 (Salt Bridge/Attractive charge)
Nitroxoline	3VOB	-6.13	32	Leu200, Gly205, Asn208, Leu209, Asn263, Thr309 (H-B), Val297 (pi-sigma), Asp199 (amide pi-stacked), Val203, Leu200, Val297 (pi-alkyl)
Compound (**3**)		-8.54	1.00	Thr309 (H-B), Val297 (pi-sigma), Leu200, Val309, Val297 (pi-alkyl)
Ciprofloxacin	1ZI0	-7.20	21	Val737, Arg739, Asp790 (H-B), Arg739, Gln788 (C-H), Ile736 (pi-sigma), Ile736, Val787 (alkyl/pi-alkyl)
Compound (**2**)		-9.08	0.22	Asp686, Arg838 (H-B), Ile736 (pi-sigma), Leu735, Val787 (pi-alkyl)

Ciprofloxacin	6F86	-7.14	3.44	
Compound (**3**)		-7.16	5.21	Asn46, Asp73, Val120 (H-B), Ile78, Thr165 (pi-sigma), Asn46 (amide-pi stacked), Ile78, Ile94 (pi-alkyl)
Ceftaroline	4CJN	-6.86	6.99	Asp586, His583, Ser643, Ala642 (H-B), His583, Glu447 (salt Bridge/Attractive charge), Ala642 (pi-alkyl)
Compound (**3**)		-8.45	0.88	Ser403, Ser462 (H-B), Gly599 (C-H), Lys406, Lys597 (salt Bridge/Attractive charge), His583 (pi-pi stacked), Ala462 (pi-alkyl)

ADMET Prediction

Based on the ADMET prediction findings evaluated with a value of 150, all compounds were determined to be effectively digested in the human intestine. Compounds **1**, **2,** and **3**, particularly with the hydroxyquinolines derived, demonstrated a potential logarithm of water solubility value range of -1.48, -1.907, and -2.153, respectively. All of the compounds were found to have a high Blood-Brain Barrier (BBB) permeability as well as except for compound **1**, and all compounds have no hepatotoxicity profile. From the result, these compounds showed no potential effect on liver damage. Moreover, Profiling the drug candidate's interaction with these enzymes is essential to recognize whether the drugs can develop toxicities or interact with another drug in the body, which results in ineffective pharmacological effects. The drug interactions with CYP450 are divided into enzyme inhibition and induction. CYP450 inhibitor reduces the metabolism activity

of this enzyme, while CYP450 inducer can act as the substrate and undergo biotransformation or increase enzyme synthesis (McDonnell & Dang, 2013; Zanger & Schwab, 2013). From the prediction using pkCSM software, all selected ligands were observed to be unable to interact with CYP450, neither as an inhibitor nor as a substrate. The hERG encodes a potassium ion channel that contributes to the electrical heart activity by repolarising the cardiac action potential. Inhibition of this channel can cause potentially fatal symptoms (Priest et al., 2008). From the prediction, all three ligands subjected to the hERG inhibitor predictor show no potential to inhibit this channel, indicating their suitability as therapeutic candidates. The information is summarized in Table 2.

Table 2. Representing ADMET properties

S. No.	A. Solubility	HIA	BBB	CYP Substrate	CYP Inhibitor	hERG	Hepatotoxicity
Compound **1**	-1.48	81.291	-0.048	No	No	No	Yes
Compound **2**	-1.907	81.966	-0.389	No	No	No	No
Compound **3**	-2.153	82.962	-0.108	No	No	No	No

Drug-likeness predictions

Compounds **1-3** followed Lipinski's rule of 5. Their logP value ranged from 0.9 to 3.71. Their respective molecular weights were less than 500 g/mol. The number of hydrogen bond donors was

C-5, C-3, and C-1 for compounds **1**, **2**, and **3**, respectively. All compounds showed a polar surface area of less than 140 $Å^2$. The number of rotatable bonds (from 2 to 4) was in the ideal range. The logS value was greater than -4 for all compounds (-4.19, -5.11, -4.81 for compounds **1**, **2**, and **3**, respectively, indicating a certain degree of flexibility for all compounds (Table 3).

Table 3. Representing Drug likeness properties

S. No	Log_p	Molecular weight (g/mol)	No. of Hydrogen bond donor	No. of Hydrogen bonds accepter	No. of Rotatable bonds	Polar Surface area ($Å^2$)	Log S
Compound **1**	3.71	391	5	6	4	118	-4.19
Compound **2**	0.9	310	3	7	3	112	-5.11
Compound **3**	3.08	327	1	6	3	124	-4.81

Molecular Dynamic Simulation

Molecular dynamics (MD) simulation studies are frequently used to verify the stability of lead-docked complexes and the binding posture acquired in docking experiments. MD simulations were performed using the Desmond (Schrödinger Maestro—Desmond Interoperability Tools) program for 100 nanoseconds (ns) time span (Roney et al., 2021). In this study, to assess such an effect, a number of parameters, including the RMSD, Root Mean Square Fluctuation (RMSF), and H-bond occupancy during simulation events of protein-ligand complexes, were explored rigorously.

Root Mean Square Deviation (RMSD) Calculations:

In MD simulation, RMSDs were measured as the deviation in the structure of protein or protein-ligand complex with respect to a reference structure, usually the initial frame. The data is shown

in Table 4. Figure 7 shows RMSD in Cα atoms of 1JIJ, 3VOB, and 1ZI0 alone (teal colour) and 1JIJ-Compound (3), 3VOB-Compound (3), and 1ZI0- Compound **2** complex (brown line). The most prominent complex overlay has been observed between 3VOB and compound **3**, as seen in figure 7(c). The figure clearly shows that throughout the MD simulation and after equilibration, the RMSD of Cα atoms fluctuated, as it peaked at 90 ns to reach 3.2 Å. Likewise, the ligand RMSD value diverges from the protein and plunges at 80 ns to reach 0.5 Å in a range between 0.4 to 3.2 Å, while the protein range was between 1.3 Å and 3.2 Å. Since the change in the protein RMSD is less than 3 Å, thus it is not undergoing a large conformational change during the simulation. According to Bhowmick et al. (2020), RMSD value ≥3 Å is very high, indicating large conformational changes in their bound states. However, the RMSD values were expected to stabilize better after equilibrium. Finally, the complex was stable until 60 ns; heavy ligand atoms are expected to have diffused away from the binding sites of the protein between 60 and 90 ns. Figure 7(a) and 7(b) of the other two protein-ligand complexes show that the equilibrium was not achieved during the 100 ns simulations. Although a sudden increase in RMSD value was noticed after 65 nanoseconds for the compound 3 bound with 3VOB protein because of the entry of a large ligand (**3**) into the substrate-binding site of the target protein; however, the changes remain stable for a more extended period till 92 nanoseconds indicating that the ligand continued to move away from the binding site of target protein, and the binding might not occur. After 92 ns, it dramatically drops to 3.2 Å, which indicates that subtle conformational change can hold a stable protein-ligand complex. The complex 1ZI0-Compound (**2**) was the most prominent example of an unstable ligand in the binding site of the protein, as the RMSD range of the protein was between 1 and 70, confirming that the fluctuation of the structure was beyond all its thermal average, which can be attributed to the large protein size compared to the other proteins tested in this study.

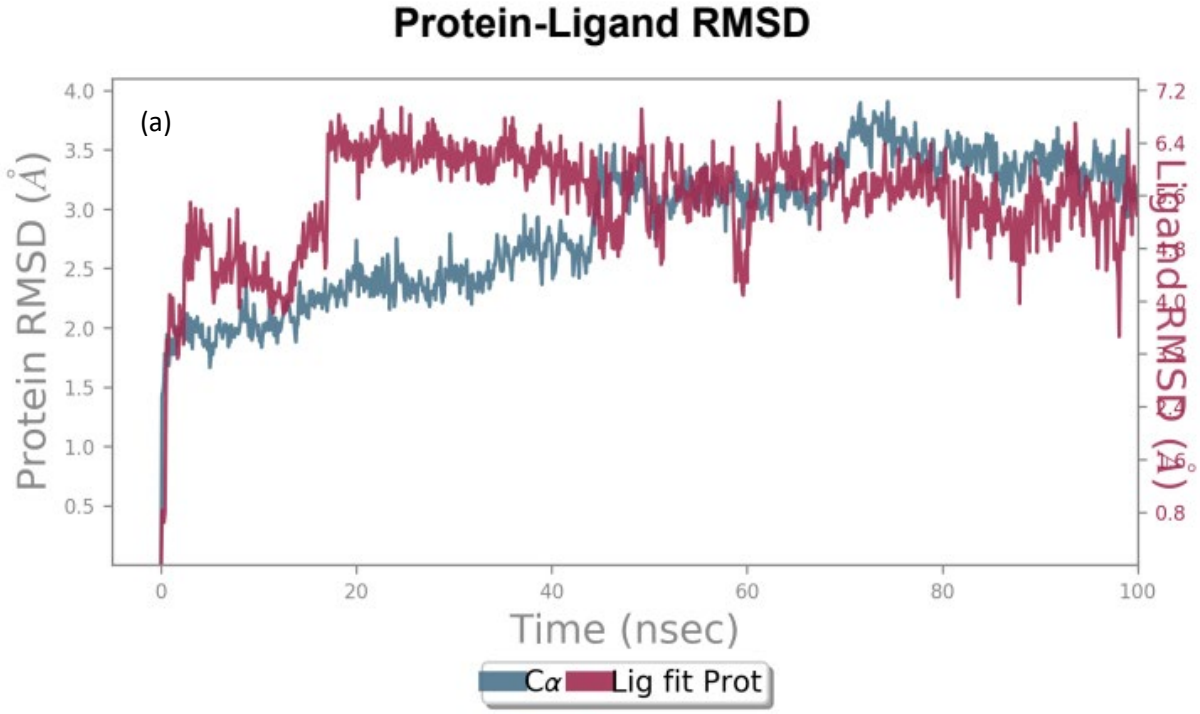
Protein-Ligand RMSD
(a)
Protein RMSD (Å)
Ligand RMSD (Å)
Time (nsec)
Cα
Lig fit Prot

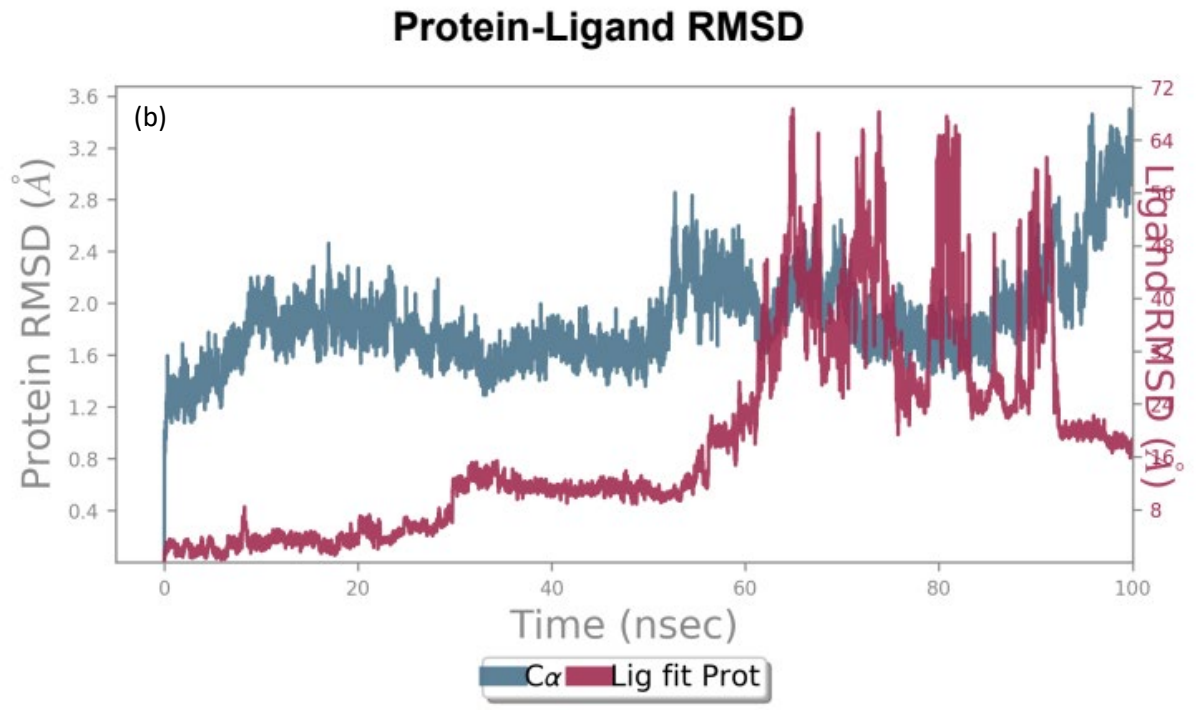
Protein-Ligand RMSD
(b)
Protein RMSD (Å)
Ligand RMSD (Å)
Time (nsec)
Cα
Lig fit Prot

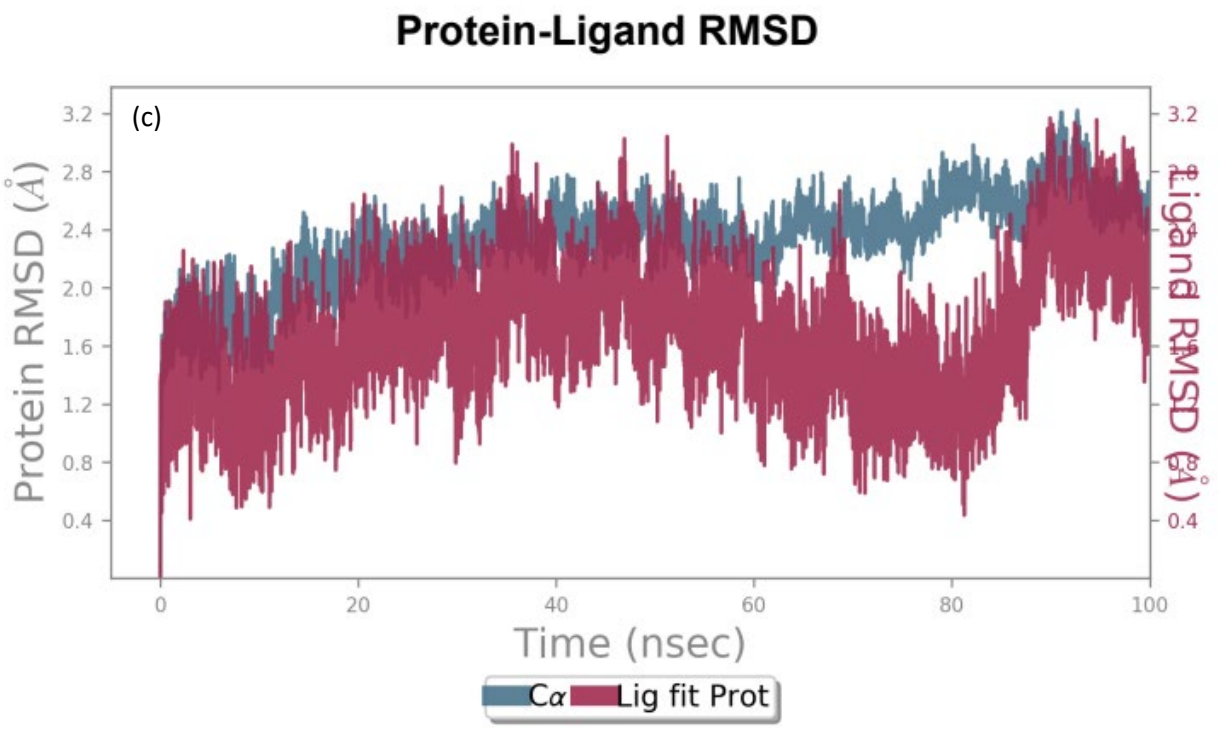

Figure 7. RMSD in Cα atoms of 1JIJ, 3VOB and 1ZI0 alone (teal colour) and 1JIJ-Compound (3), 3VOB-Compound (3) and 1ZI0- Compound (2) complex (brown line)

Root Mean Square Fluctuation (RMSF) Calculations

In MD simulation, the RMSF value of a protein is generally measured to assess the fluctuations in the side chains due to the binding of a ligand, in addition to determining the complex's conformational flexibility. Figure 8 depicted the RMSF of target proteins 1JIJ, 3VOB, and 1ZI0 (teal colour) in the presence of compound (**3**), Compound (**3**), and Compound (**2**), respectively, during the MD simulation and compared it with the experimentally determined B-factor (red colour) obtained during X-ray crystallography. The statistics clearly show that the variations are pretty minor in the 3VOB and 1JIJ with their respective ligands. For Cα atoms, the RMSF ranges from 0.5 Å to 4.80 Å figure 8(a) and from 0.4 Å to 3.60 Å figure 8(c). The ligand atoms (Figure 8(c)) display a fluctuation of about 0.75 Å, and a fluctuation of 3.9 Å in 1JIJ- compound (**3**) can

be considered acceptable RMSF values. These findings indicate that the combination is stable, and its structural flexibility is limited in 3VOB and 1JIJ complexes. Moreover, major fluctuation in RMSF values of 1ZIO side chains might have been due to the entry and binding of compound **2** into the groove of the target protein, which is about 22 Å and 5.0 Å (Figure 8(b)). The data is shown in Table 4.

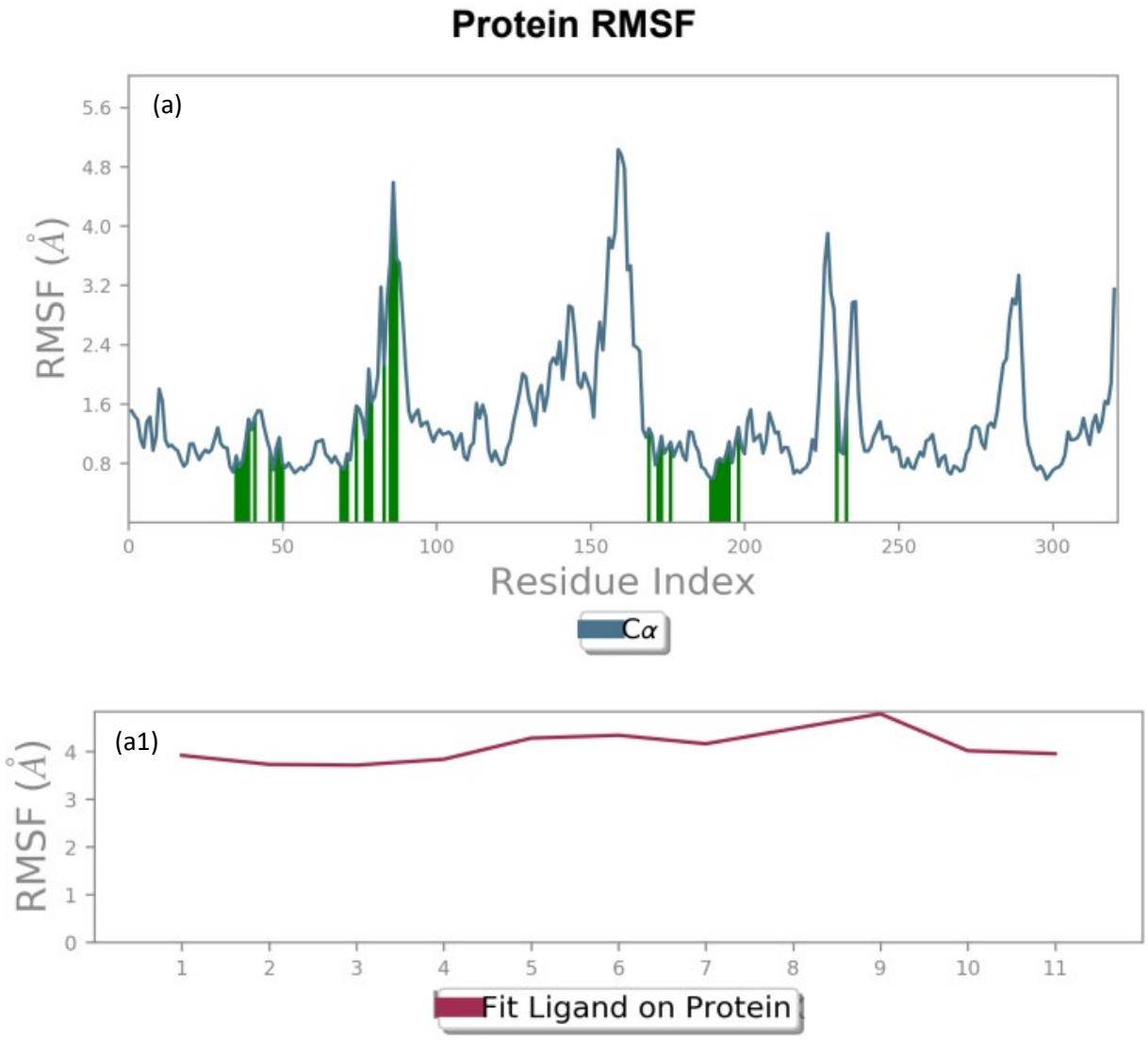

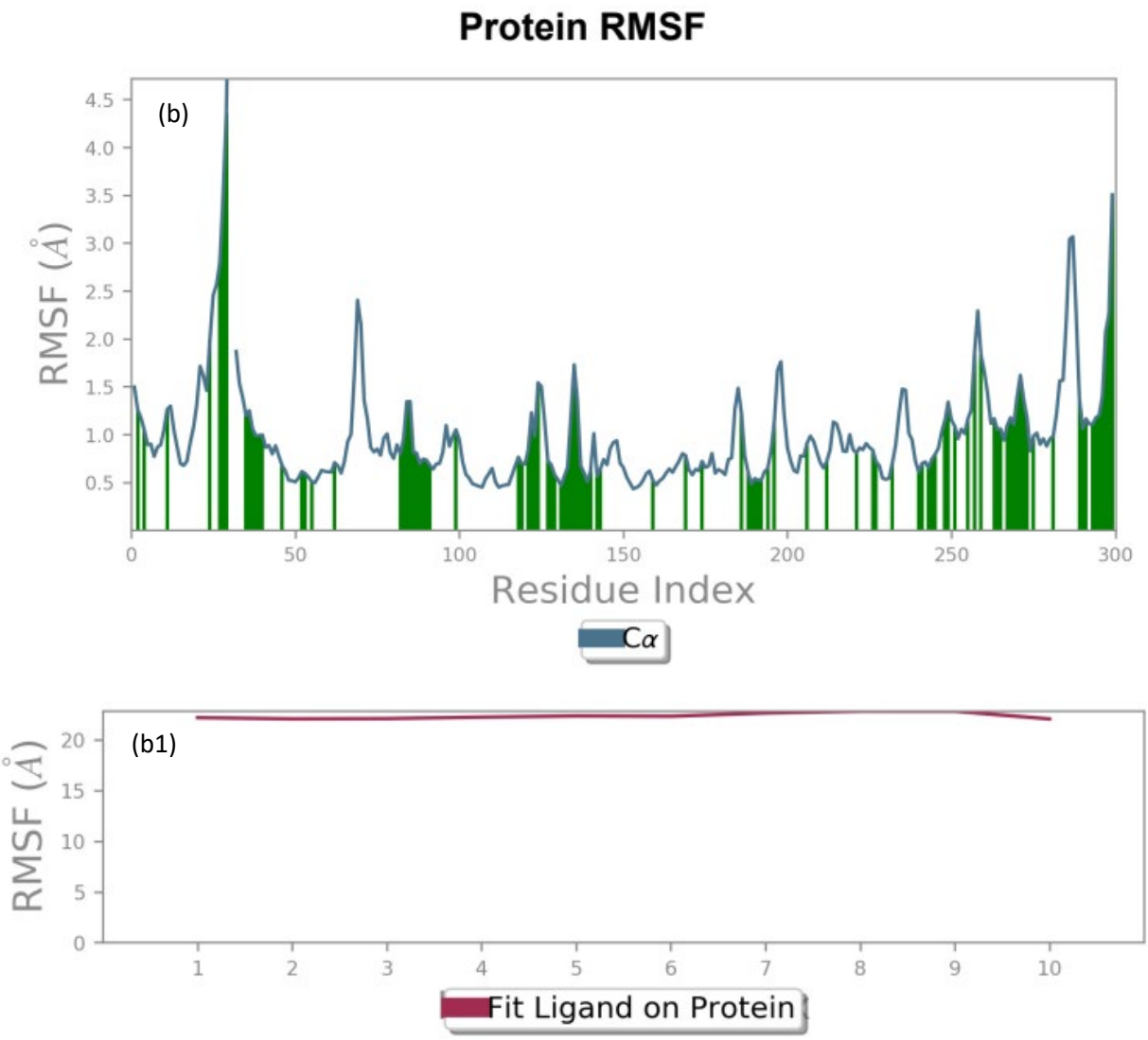
Protein RMSF
(b)
RMSF (Å)
4.5
4.0
3.5
3.0
2.5
2.0
1.5
1.0
0.5
0
50
100
150
200
250
300
Residue Index
Cα
(b1)
RMSF (Å)
20
15
10
5
0
1
2
3
4
5
6
7
8
9
10
Fit Ligand on Protein

(b1)

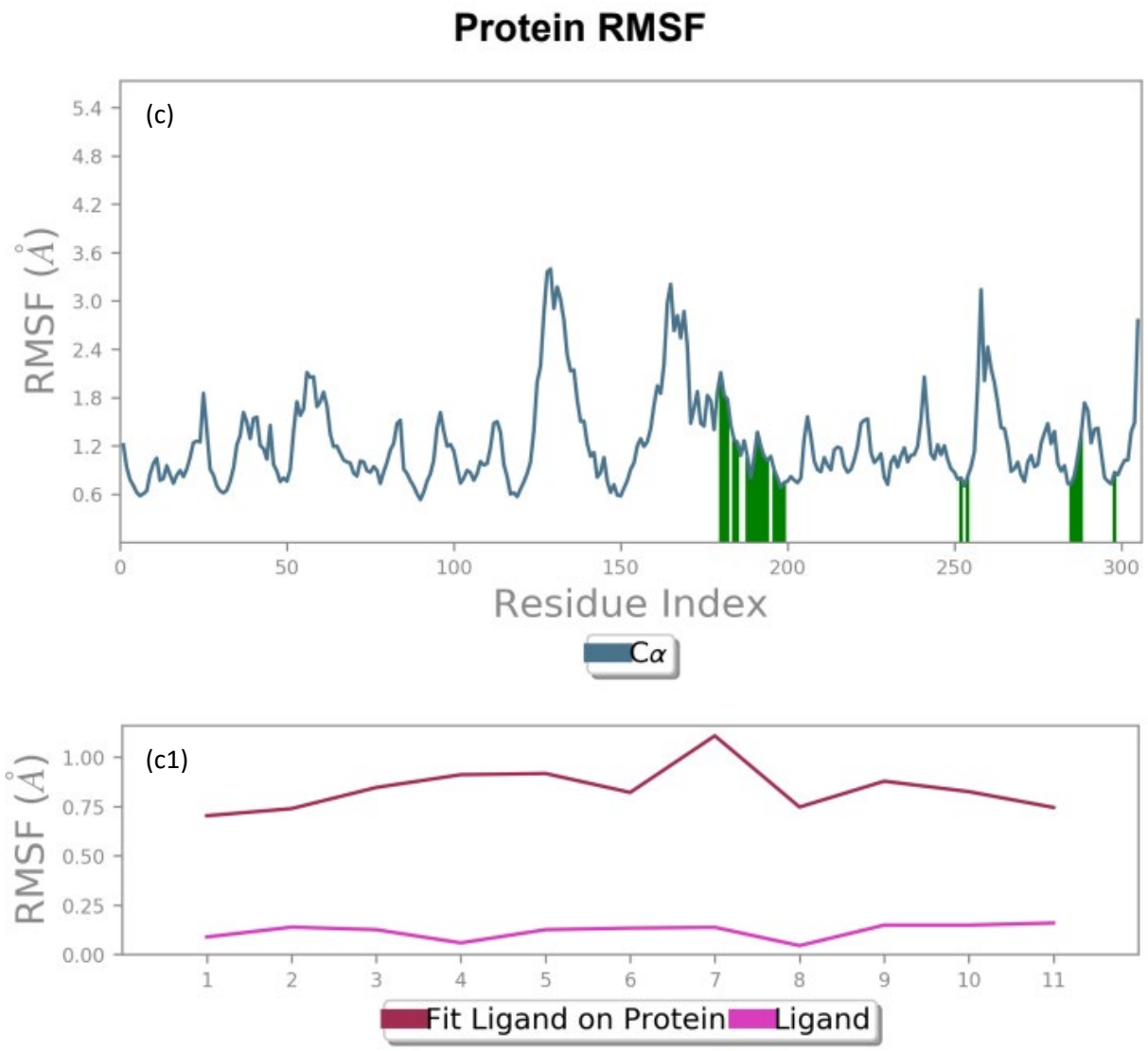

(c1)

Figure 8. The RMSF of target proteins 1JIJ, 3VOB, and 1ZI0 (teal colour) in the presence of compound (**3**), Compound (**3**), and Compound (**2**), respectively

Protein-ligand H-B (Hydrogen Bonds) analysis

The total number of H-B between the target proteins and selected compounds during the simulations was determined to be very in the 4-20 range, with 11 H-B for 1JIJ-compound (3), 6 H-B for 3VOB-compound (3) and 9 H-B for 1ZI0- compound (2) complex (Figure 9). Moreover,

the involvement of amino acid residue in making contact with compound **3** during the simulation for 1JIJ showed that Gly38, Ala39, His50, Leu70, Tyr170, Gln174, Asp177, Gln190, Gln196, Asn199, and Lys231 were involved in making contact for most of the simulation (Figure 9C). Likewise, H-B for 3VOB-compound **3** showed interactions with Gln195, Gln196, Asp199, Gly205, Leu209, and Asn263 amino acid residues, as well as 1ZI0- compound (2) complex showed the H-B with the residues of Thr542, Tyr548, Lys550, Asp576, Ile578, Arg615, Val659, Ala713, and Glu841. The data is shown in Table 4.

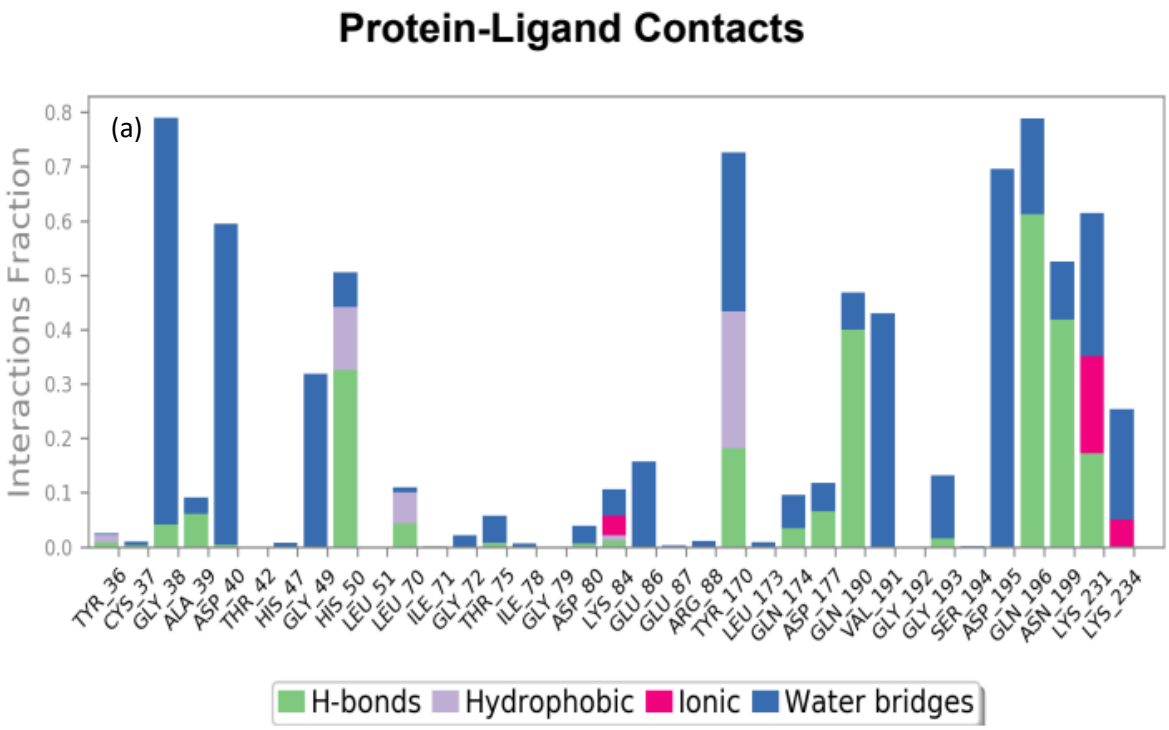

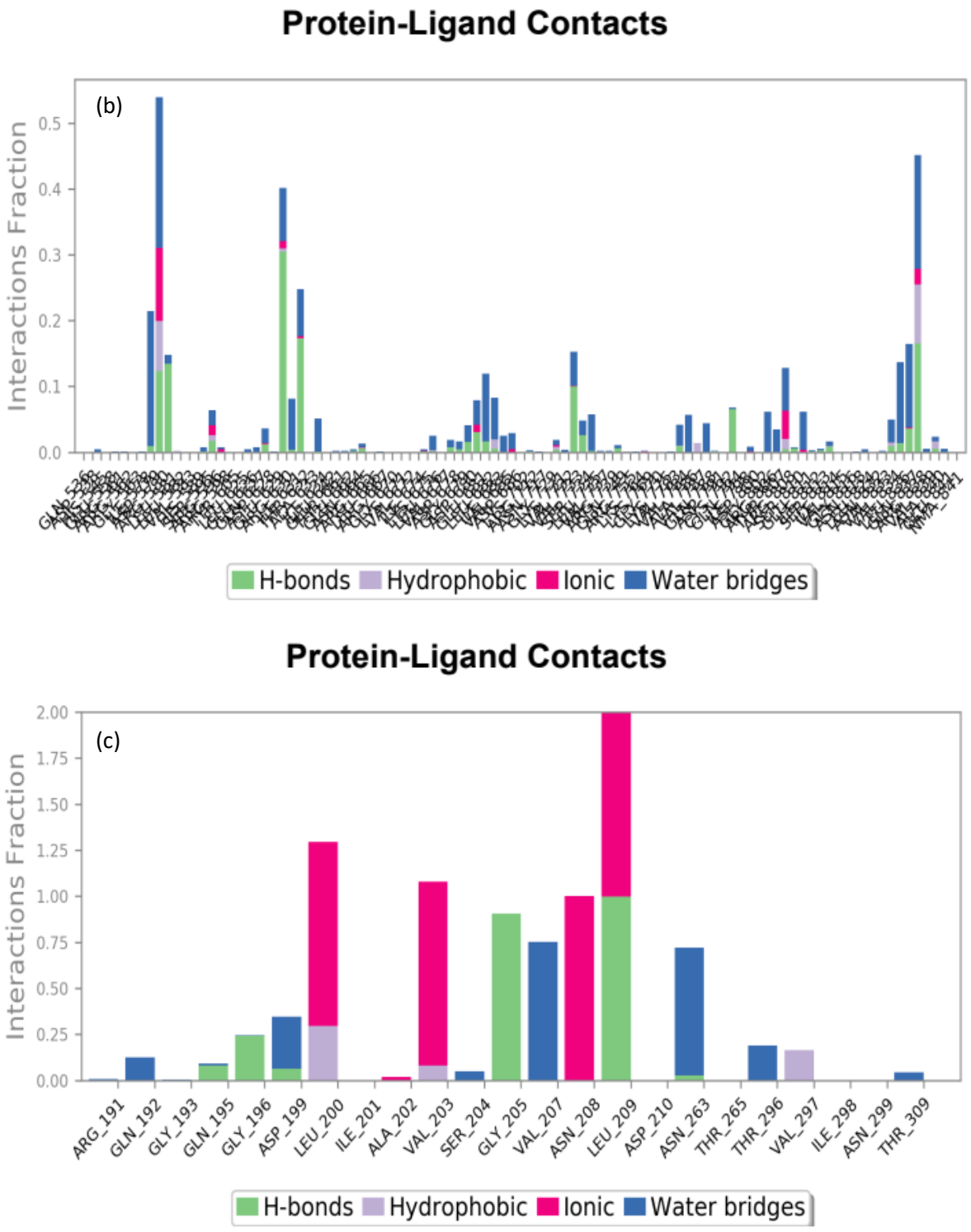

Figure 9. H-B between the target proteins and selected compounds.

Table 4. RMSD and RMSF of protein-ligand complexes and ligands

Complex	Protein RMSD	Ligand RMSD	Protein RMSF	Ligand RMSF	H-B
1JIJ-Compound (3)	3.2 Å	5.4 Å	0.75 Å	3.9 Å	Gly38, Ala39, His50, Leu70, Tyr170, Gln174, Asp177, Gln190, Gln196, Asn199, Lys231
3VOB-Compound (3)	1.3 Å	3.2 Å	0.5 Å	4.8 Å	Gln195, Gln196, Asp199, Gly205, Leu209, Asn263
1ZI0-Compound (2)	3.6 Å	16 Å	5.0 Å	22 Å	Thr542, Tyr548, Lys550, Asp576, Ile578, Arg615, Val659, Ala713, Glu841

Molecular mechanics generalized Born surface area (MM/GBSA) calculations

The MD simulation trajectories calculated the binding free energy of proposed molecules and proteins using the MM-GBSA approach. It is illustrated that binding energy computed using the MMGBSA method can be considered more accurate than the Glide score value for any protein-ligand complex. Here, the greater the negative free energies of binding value, the stronger the binding among the ligand compound with the targeted protein complex (Table 5). The findings strongly depicted that compound **2** with 1ZIO protein complex possessed strong binding free energy -36.80. In contrast, compound **3** with 1JIJ protein complex and compound **3** with 3VOB protein complex have been shown the binding free energy -14.88 and -10.73 consecutively.

Therefore, based on the free binding energy calculations, the selected compounds were deduced with considerable binding affinity for the target proteins and concluded the proposed molecules as potential anti-bacterial.

Table 5. MM/GBSA Calculation by Maestro Application of Schrodinger Package Software

Protein ID	**Ligand PubChem CID**	**MM/GBSA ΔG Bind Score (Kcal/Mol)**
1ZIO	Compound **2**	-36.8001488
1JIJ	Compound **3**	-14.88156648
3VOB	Compound **3**	-10.73100391

Conclusion

Bacterial infections caused by drug-resistant strains have become more challenging to treat, and there is an urgent need to identify chemical scaffolds with new modes of action. Our molecular docking study identified two hydroxyquinoline derivatives with a high binding affinity towards the active sites of five bacterial proteins. These compounds may serve as potential new drug templates to combat infections caused by bacterial strains, particularly the Gram-positive *S. aureus* (including MRSA) and the Gram-negative *E. coli.* Their relatively easy synthesis (azo coupling reaction of hydroxyquinoline with the diazonium salt of either sulfanilamide (**1**) or sulfanilic acid (**3**)) is likely to help further investigations, including experimental *in vitro* and *in vivo* studies.

Supplementary Materials: The following are available online at the journal website, Supplementary Table S1-S11.

Author Contributions: Conceptualization, M.S.H and Y.A.; methodology, F.R., S.M., M.R., Y.A. and S.Q.; software, Y.A.; validation, Y.A., M.S.H., M.R., R.M., and V.S.; formal analysis, F.R. and S.Q.; investigation, F.R.; M.R. and S.Q.; resources, Y.A.; data curation, F.R., M.S.H.,

M.R. and S.Q.; writing—original draft preparation, F.R., S.Q., Y.A., and M.S.H.; writing—review and editing, M.S.H., M.R.; S.M., R.M. R.A.H, H.U.R., V.S., and L.C.M.; visualization, F.R. and S.Q., M.R. and S.M.; supervision, Y.A., R.M. and M.S.H.; project administration, Y.A. All authors have read and agreed to the published version of the manuscript.

Acknowledgements: The authors are thankful to the Sarhad University of Science and Information Technology, Peshawar, Pakistan, for providing resources for this study.

Conflicts of Interest: The authors declare no conflict of interest.

References

Abdullah, M. I., Mahmood, A., Madni, M., Masood, S., & Kashif, M. (2014). Synthesis, characterization, theoretical, anti-bacterial and molecular docking studies of quinoline based chalcones as a DNA gyrase inhibitor. *Bioorg Chem, 54*, 31-37. doi:10.1016/j.bioorg.2014.03.006

Adams, D. W., & Errington, J. (2009). Bacterial cell division: assembly, maintenance and disassembly of the Z ring. *Nature Reviews Microbiology, 7*(9), 642-653.

Berry, M. B., & Phillips, G. N., Jr. (1998). Crystal structures of Bacillus stearothermophilus adenylate kinase with bound Ap5A, Mg2+ Ap5A, and Mn2+ Ap5A reveal an intermediate lid position and six coordinate octahedral geometry for bound Mg2+ and Mn2+. *Proteins, 32*(3), 276-288.

Bhowmick, S., Alissa, S. A., Wabaidur, S. M., Chikhale, R. V., & Islam, M. A. (2020). Structure-guided screening of chemical database to identify NS3-NS2B inhibitors for effective therapeutic application in dengue infection. *J Mol Recognit, 33*(7), e2838. doi:10.1002/jmr.2838

Bouzian, Y., Karrouchi, K., Sert, Y., Lai, C.-H., Mahi, L., Ahabchane, N. H., . . . Essassi, E. M. (2020). Synthesis, spectroscopic characterization, crystal structure, DFT, molecular docking and in vitro antibacterial potential of novel quinoline derivatives. *Journal of Molecular Structure, 1209*, 127940.

Bouzian, Y., Karrouchi, K., Sert, Y., Lai, C. H., Mahi, L., Ahabchane, N. H., . . . Essassi, E. (2020). Synthesis, spectroscopic characterization, crystal structure, DFT, molecular docking and in vitro antibacterial potential of novel quinoline derivatives. *Journal of Molecular Structure, 1209*, 127940. doi:10.1016/j.molstruc.2020.127940

Breijyeh, Z., Jubeh, B., & Karaman, R. (2020). Resistance of Gram-negative bacteria to current antibacterial agents and approaches to resolve it. *Molecules, 25*(6), 1340.

Cherdtrakulkiat, R., Boonpangrak, S., Sinthupoom, N., Prachayasittikul, S., Ruchirawat, S., & Prachayasittikul, V. (2016). Derivatives (halogen, nitro and amino) of 8-hydroxyquinoline with highly potent antimicrobial and antioxidant activities. *Biochem Biophys Rep, 6*, 135-141. doi:10.1016/j.bbrep.2016.03.014

El Faydy, M., Djassinra, T., Haida, S., Rbaa, M., Ounine, K., Kribii, A., & Lakhrissi, B. (2017). Synthesis and investigation of antibacterial and antioxidants properties of some new 5-subsituted-8-hydroxyquinoline derivatives. *J. Mater. Environ. Sci, 8*(11), 3855-3863.

Enquist, P. A., Gylfe, A., Hagglund, U., Lindstrom, P., Norberg-Scherman, H., Sundin, C., & Elofsson, M. (2012). Derivatives of 8-hydroxyquinoline--antibacterial agents that target intra- and extracellular Gram-negative pathogens. *Bioorganic & medicinal chemistry letters, 22*(10), 3550-3553. doi:10.1016/j.bmcl.2012.03.096

Ezeokonkwo, M. A., Ibeanu, F., Eze, C., Ibezim, A., Ezeokoye, C., Ezenwa, O., . . . Vincent, O. (2019). Synthesis, antimi-crobial activity and molecular docking studies of 7-bromoquinoline-5, 8-dione containing aryl sulphonamides. *Int. J. Appl. Chem, 15*, 99-112.

Faydy, M. E., Dahaieh, N., Ounine, K., Rastija, V., Almalki, F., Jamalis, J., . . . Lakhrissi, B. (2021). Synthesis and antimicrobial activity evaluation of some new 7-substituted quinolin-8-ol derivatives: POM analyses, docking, and identification of antibacterial pharmacophore sites. *Chemical Data Collections, 31*, 100593. doi:10.1016/j.cdc.2020.100593

Genheden, S., & Ryde, U. (2010). How to obtain statistically converged MM/GBSA results. *Journal of computational chemistry, 31*(4), 837-846.

Godschalk, F., Genheden, S., Soderhjelm, P., & Ryde, U. (2013). Comparison of MM/GBSA calculations based on explicit and implicit solvent simulations. *Phys Chem Chem Phys, 15*(20), 7731-7739. doi:10.1039/c3cp00116d

Gupta, M., Sharma, R., & Kumar, A. (2018). Docking techniques in pharmacology: How much promising? *Computational biology and chemistry, 76*, 210-217.

Gupta, P., Mohammad, T., Dahiya, R., Roy, S., Noman, O. M. A., Alajmi, M. F., . . . Hassan, M. I. (2019). Evaluation of binding and inhibition mechanism of dietary phytochemicals with sphingosine kinase 1: Towards targeted anticancer therapy. *Sci Rep, 9*(1), 18727. doi:10.1038/s41598-019-55199-3

Hossain, M. S., Sharfaraz, A., Dutta, A., Ahsan, A., Masud, M. A., Ahmed, I. A., . . . Ming, L. C. (2021). A review of ethnobotany, phytochemistry, antimicrobial pharmacology and toxicology of Nigella sativa L. *Biomed Pharmacother, 143*, 112182. doi:10.1016/j.biopha.2021.112182

Hossain, S., Urbi, Z., Karuniawati, H., Mohiuddin, R. B., Moh Qrimida, A., Allzrag, A. M. M., . . . Capasso, R. (2021). Andrographis paniculata (Burm. f.) Wall. ex Nees: An Updated Review of Phytochemistry, Antimicrobial Pharmacology, and Clinical Safety and Efficacy. *Life (Basel), 11*(4). doi:10.3390/life11040348

Jin, G., Xiao, F., Li, Z., Qi, X., Zhao, L., & Sun, X. (2020). Design, Synthesis, and Dual Evaluation of Quinoline and Quinolinium Iodide Salt Derivatives as Potential Anticancer and Antibacterial Agents. *ChemMedChem, 15*(7), 600-609. doi:10.1002/cmdc.202000002

Joaquim, A. R., Reginatto, P., Lopes, M. S., Bazana, L. C. G., Gionbelli, M. P., de Cesare, M. A., . . . de Andrade, S. F. (2021). New 8-hydroxyquinoline derivatives highlight the potential of this class for treatment of fungal infections. *New Journal of Chemistry, 45*(38), 18158-18170. doi:10.1039/d0nj06188c

Karuniawati, H., Hassali, M. A. A., Suryawati, S., Ismail, W. I., Taufik, T., & Hossain, M. S. (2021). Assessment of Knowledge, Attitude, and Practice of Antibiotic Use among the Population of Boyolali, Indonesia: A Cross-Sectional Study. *Int J Environ Res Public Health, 18*(16). doi:10.3390/ijerph18168258

Kouznetsov, V. V., Mendez, L. Y. V., Galvis, C. E. P., & Villamizar, M. C. O. (2020). The direct C-H alkenylation of quinoline N-oxides as a suitable strategy for the synthesis of promising antiparasitic drugs. *New Journal of Chemistry, 44*(1), 12-19. doi:10.1039/c9nj05054j

Kumar, T. O., Mahadevan, K. M., Ganapathy, P. S., & Kumara, M. N. (2015). Synthesis and molecular docking study of 2-aryl/heteroaryl-6chloroquinoline-4-carboxylic acids with plasmodium LDH receptor protein. *Int J Pharm Pharm Sci, 7*(1), 431-437.

Kumar, V., Tang, C., Bethel, C. R., Papp-Wallace, K. M., Wyatt, J., Desarbre, E., . . . van den Akker, F. (2020). Structural Insights into Ceftobiprole Inhibition of Pseudomonas aeruginosa Penicillin-Binding Protein 3. *Antimicrobial agents and chemotherapy, 64*(5), e00106-00120. doi:10.1128/AAC.00106-20

Lam, K. H., Gambari, R., Lee, K. K., Chen, Y. X., Kok, S. H., Wong, R. S., . . . Chui, C. H. (2014). Preparation of 8-hydroxyquinoline derivatives as potential antibiotics against Staphylococcus aureus. *Bioorganic & medicinal chemistry letters, 24*(1), 367-370. doi:10.1016/j.bmcl.2013.10.072

Le, T. D., Pham, N. N., & Nguyen, T. C. (2018). Preparation and Antibacterial Activity of Some New 4-(2-Heterylidenehydrazinyl)-7-chloroquinoline Derivatives. *Journal of Chemistry, 2018*, 1-7. doi:10.1155/2018/4301847

Liang, J., Tan, P., Zhao, Y., Li, L., Jin, S., Hong, L., & Xu, Z. (2021). Super-scalable molecular dynamics algorithm. *arXiv preprint arXiv:2106.05494*.

Mandewale, M. C., Thorat, B., Patil, U., Kale, B., & Yamgar, R. (2015). Developments in quinoline synthesis: a review. *Heterocyclic Letters, 5*(5), 475-488.

McDonnell, A. M., & Dang, C. H. (2013). Basic review of the cytochrome p450 system. *J Adv Pract Oncol, 4*(4), 263-268. doi:10.6004/jadpro.2013.4.4.7

Mustafa, Y. F. (2018). Synthesis, characterization and antibacterial activity of novel heterocycle, coumacine, and two of its derivatives. *Saudi Pharm J, 26*(6), 870-875. doi:10.1016/j.jsps.2018.03.010

Muthukumar, K., Velmurugan, K., & Derin, T. D. (2019). Synthesis, characterization, antibacterial and antioxidant studies of oxetoquinolines. *MOJ Biorg Org Chem, 3*(2), 38-43.

Nakajima, T., Kajikawa, Y., Hirose, T., Tokiwa, N., Hanada, K., & Fukuhara, T. (1978). Surgical-orthodontic approach to skeletal class III malocclusion. Analysis of 45 cases with evaluation of curved oblique osteotomy and sliding osteotomy. *Int J Oral Surg, 7*(4), 274-280. doi:10.1016/s0300-9785(78)80094-5

Narramore, S., Stevenson, C. E. M., Maxwell, A., Lawson, D. M., & Fishwick, C. W. G. (2019). New insights into the binding mode of pyridine-3-carboxamide inhibitors of E. coli DNA gyrase. *Bioorganic & medicinal chemistry, 27*(16), 3546-3550. doi:10.1016/j.bmc.2019.06.015

Neupane, N. P., Kushwaha, A. K., Karn, A. K., Khalilullah, H., Khan, M. M. U., Kaushik, A., & Verma, A. (2022). Anti-bacterial efficacy of bio-fabricated silver nanoparticles of aerial part of Moringa oleifera lam: Rapid green synthesis, In-Vitro and In-Silico screening. *Biocatalysis and Agricultural Biotechnology, 39*, 102229.

Oh, K. J., & Klein, M. L. (2006). A general purpose parallel molecular dynamics simulation program. *Computer physics communications, 174*(7), 560-568.

Oliva, M. A., Cordell, S. C., & Löwe, J. (2004). Structural insights into FtsZ protofilament formation. *Nature structural & molecular biology, 11*(12), 1243-1250.

Priest, B. T., Bell, I. M., & Garcia, M. L. (2008). Role of hERG potassium channel assays in drug development. *Channels (Austin), 2*(2), 87-93. doi:10.4161/chan.2.2.6004

Qiu, X., Janson, C. A., Smith, W. W., Green, S. M., McDevitt, P., Johanson, K., . . . Jarvest, R. L. (2001). Crystal structure of Staphylococcus aureus tyrosyl-tRNA synthetase in complex with a class of potent and specific inhibitors. *Protein Sci, 10*(10), 2008-2016. doi:10.1110/ps.18001

Rbaa, M., Hichar, A., Bazdi, O., Lakhrissi, Y., Ounine, K., & Lakhrissi, B. (2019). Synthesis, characterization, and in vitro antimicrobial investigation of novel pyran derivatives based on 8-hydroxyquinoline. *Beni-Suef University Journal of Basic and Applied Sciences, 8*(1), 8. doi:10.1186/s43088-019-0009-9

Rbaa, M., Jabli, S., Lakhrissi, Y., Ouhssine, M., Almalki, F., Ben Hadda, T., . . . Lakhrissi, B. (2019). Synthesis, antibacterial properties and bioinformatics computational analyses of novel 8-hydroxyquinoline derivatives. *Heliyon, 5*(10), e02689. doi:10.1016/j.heliyon.2019.e02689

Roney, M., Huq, A. K. M. M., Rullah, K., Abd Hamid, H., Imran, S., Islam, M. A., & Aluwi, M. F. F. M. (2021). Virtual Screening-Based Identification of Potent DENV-3 RdRp Protease Inhibitors via In-House Usnic Acid Derivative Database. *Journal of Computational Biophysics and Chemistry, 20*(08), 797-814. doi:10.1142/S2737416521500496

Sashidhara, K. V., Avula, S. R., Mishra, V., Palnati, G. R., Singh, L. R., Singh, N., . . . Bhatta, R. S. (2015). Identification of quinoline-chalcone hybrids as potential antiulcer agents. *Eur J Med Chem, 89*, 638-653.

Sharma, R., Kour, P., & Kumar, A. (2018). A review on transition-metal mediated synthesis of quinolines. *Journal of Chemical Sciences, 130*(6), 73. doi:10.1007/s12039-018-1466-8

Solomon, S. L., & Oliver, K. B. (2014). Antibiotic resistance threats in the United States: stepping back from the brink. *Am Fam Physician, 89*(12), 938-941.

Thiede, J. M., Kordus, S. L., Turman, B. J., Buonomo, J. A., Aldrich, C. C., Minato, Y., & Baughn, A. D. (2016). Targeting intracellular p-aminobenzoic acid production potentiates the anti-tubercular action of antifolates. *Sci Rep, 6*(1), 38083. doi:10.1038/srep38083

Tjampakasari, C. R., Kalisya, N. A., & Sudiro, T. M. (2021). Description of Methicilin-Sensitive Staphylococcus aureus (MSSA) and Methicilin-Resistant Staphylococcus aureus (MRSA) against Fluoroquinolone and Vancomycin Group Antibiotics in Jakarta. *Indonesian Journal of Biotechnology and Biodiversity, 5*(5), 48-52.

Urbi, Z., Azmi, N. S., & Hossain, M. S. (2021). *Antimicrobial Role of Glycosaminoglycans: Beyond Bacterial Adhesion to Host Cell*. Paper presented at the The 1st International Electronic Conference on Antibiotics, Basel, Switzerland. https://sciforum.net/paper/view/9917

WHO. (2020). Antibiotic resistance. Retrieved from https://www.who.int/news-room/fact-sheets/detail/antibiotic-resistance

Zanger, U. M., & Schwab, M. (2013). Cytochrome P450 enzymes in drug metabolism: regulation of gene expression, enzyme activities, and impact of genetic variation. *Pharmacol Ther, 138*(1), 103-141. doi:10.1016/j.pharmthera.2012.12.007

Zeleke, D., Eswaramoorthy, R., Belay, Z., & Melaku, Y. (2020). Synthesis and Antibacterial, Antioxidant, and Molecular Docking Analysis of Some Novel Quinoline Derivatives. *Journal of Chemistry, 2020*, 1324096. doi:10.1155/2020/1324096